Supplementary Materials

Cr-dopant Induced Crystal Orientation and Shape Modulation in Ni_2P Nanocrystals For Improving Electrosynthesis of Methanol to Formate Coupled with Hydrogen Production

Umesh P. Suryawanshi[a], Uma V. Ghorpade[b], Jodie A. Yuwon[c], Priyank V. Kumar[b], Mayur A. Gaikwad[a], Seung Wook Shin[d], Jun Sung Jang[a], Hyo Rim Jung[a], Mahesh P. Suryawanshi[c,], Jin Hyeok Kim [a,*]*

[a]Optoelectronics Convergence Research Center and Department of Materials Science and Engineering, Chonnam National University, 300, Yongbong-Dong, Buk-Gu, Gwangju 61186, South Korea

[b]School of Chemical Engineering, University of New South Wales, Sydney, NSW, 2052 Australia

[c]School of Chemical Engineering, the University of Adelaide, Adelaide, SA, 5005 Australia

[d]Rural Research Institute, Korea Rural Community Corporation, 870 Haean-ro Sangnok-gu, Ansan-Si, Gyeonggi-di, 15634, Republic of Korea.

[e]School of Photovoltaic and Renewable Energy Engineering, University of New South Wales, Sydney, NSW 2052, Australia

Corresponding authors

*Mahesh P. Suryawanshi (m.suryawanshi@unsw.edu.au)

*Jin Hyeok Kim (jinhyeok@chonaam.ac.kr)

TEL: +82-62-530-1709, Fax: +82-62-530-1699

Experimental section

Chemicals and materials: Nickel (II) acetate tetrahydrate ($Ni(CH_3CO_2)_2 \cdot 4\ H_2O$, $Ni(acac)_2$), Chromium hexacarbonyl $Cr(CO)_6$, Chromium nitrate ($Cr(NO_3)_3$), 1-octadecene (ODE), oleylamine (OAm) and tri-n-octylphosphine (TOP), *n*-Hexane, ethanol, methanol (MeOH) and 5 wt % nafion solution were purchased from Sigma Aldrich. All of the chemicals were used as receive without any further purification.

Synthesis of $Ni_{2-x}Cr_xP$ NCs: In a typical synthesis, $Ni(acac)_2$ (1, 0.9, 0.8, 0.7 and 0.6 mmol) and $Cr(CO)_6$ (0, 0.1, 0.2, 0.3 and 0.4 mmol) was added to a 100-mL three-necked, round bottom flask containing a borosilicate stir bar and equipped with thermocouple and rubber septum. Prior to sealing the flask, 1-ODE (9.4 mmol), OAm (13 mmol), and TOP (8.99 mmol) were added to the vessel. The reaction mixture was moderately stirred and heated, using a heating mantle, at 120 °C for 1 h under vacuum, to remove water and other low-boiling impurities. The solution was then heated at 320 °C for 4 h in an Ar atmosphere. After holding the solution at above mentioned parameters, the reaction was cooled slowly by turning off the heating mantle until the solution reached 200 °C. The flask was then removed from the heating mantle to effect rapid cooling to room temperature. The contents of the reaction mixture were transferred into centrifuge tubes equipped with caps, followed by centrifugation at 3000 rpm for 10 min. The resultant NCs was washed 3 times using 1:3 (V:V) hexane:ethanol and then was dispersed in *n*-hexane for further use. To synthesize undoped Ni_2P NCs, similar reaction process was followed except the addition of chromium precursor into reaction bath and keeping all other reaction conditions and purification steps same.

Materials characterizations

The surface morphologies were studied using high-resolution Transmission electron microscopy (HR-TEM, JEOL-3010) with an accelerating voltage of 300 kV located at Korea Institute of Basic Sciences (KBSI), Gwangju, South Korea. $Ni_{2-x}Cr_xP$ NCs, dispersed in toluene, are drop casted onto carbon meshed nickel grid for TEM sampling. The elemental distribution and compositional information were investigated by energy dispersive X-ray spectroscopy (EDS, OXFORD INCA system) using A Technai G2 F30 equipped with FE-SEM. The structural properties of the material were analyzed by the X-ray diffraction (XRD), using a XRD, PANalytical, X'Pert-PRO Netherland operated at 45 kV, 40 mA, and room temperature. A high-resolution X-ray photoelectron spectroscopy (HR-XPS, VG Multi lab 2000, Thermo VG Scientific, UK) at room temperature.

Electrochemical characterizations

All electrochemical performances of the samples were evaluated by using an Autolab potentiostat (CHI Instruments, USA) at room temperature. In a conventional three electrode system, the as-prepared electrocatalysts were used as a working electrode with the graphite rod as a counter electrode and saturated Ag/AgCl in 3.5 M KCl (0.209 V vs. NHE) was used as the reference electrode. To prepare the working electrode, 10 mg of catalysts, 50 µL of Nafion solutions were dispersed in toluene (5 mL) followed by ultrasonication for at least 2 h to form homogeneous catalyst ink. Then the catalyst ink was loaded on Ni foam with a mass loading of 5 mg/cm. An aqueous electrolyte containing 1.0 M KOH (pH = 14) was used for the HER and 1.0 M KOH/3 M methanol was used for MOR electrochemical measurements. Prior to the measurement, the aqueous electrolyte was treated with N_2 for 30 min. to remove the dissolved

oxygen (O_2) species in the solution. All the potentials reported were converted with respect to a reversible hydrogen electrode (RHE) using the following standard Nernst equation.

$$E_{RHE} = E_{Ag/AgCl} + 0.05916 \times pH + E° \quad (1)$$

where, E_{RHE} is the potential vs. RHE, $E_{Ag/AgCl}$ is the potential measured vs. Ag/AgCl and $E°_{Ag/AgCl}$ = 0.198 V at room temperature.

Linear sweep voltammetry (LSV) curves were recorded at different scan rate (5 mV s^{-1}). Electrochemical impedance spectroscopy (EIS) was performed in same electrochemical configuration and electrolyte under the dark condition on an Autolab PGSTAT equipped with an FRA2 frequency response analyzer with Nova 1.7 controlled data acquisition under open-circuit voltage. The EIS measurements were carried out in potentiostat mode at open circuit potential in the frequency range from 0.1 Hz to 10 kHz with an amplitude of ±10 mV. Each EIS spectrum were modeled using the suggested equivalent circuit by using the Z view program with relative errors below 5%. Cyclic voltammograms (CVs) were recorded at different scan rates (2, 4, 6, 8, 10 mV s^{-1}) to estimate the double-layer capacitance (C_{dl}). A chronopotentiometric measurements were conducted to test the stability of $Ni_{2-x}Cr_xP$ NCs electrocatalysts at constant current density of 10 mA/cm^2 and in a fixed potential window, respectively.

Efficiency of electrolysis

Electrolysis requires electical power as a input and generate chemical fuel as output, such as H_2(g) and O_2(g). Thus, considering that all of the current is obtained from faradaic processes (ε_{elec} = 1), the efficiency is:

$$\eta_{electrolyzer} = E_{f,a} / V_{e,i}$$

where, $E_{f,a}$ = 1.23 V; $V_{e,i}$ = input voltage required to drive the electrolysis.[1]

Density functional theory (DFT) calculations

Spin-polarized DFT calculations were implemented using the Vienna ab-initio simulation package (VASP)[2, 3] with the core and valence electronic interactions being modeled using the projector augmented wave (PAW) method.[4, 5] The Perdew-Burke-Ernzerhof (PBE) exchange-correlation function was employed.[6] The wavefunction was expanded with a kinetic energy cut-off of 500 eV and Gamma k-points were used. The Gamma k-points of 3×5×1 was used for sampling the Brillouin zone for (111) and (300) Ni_2P surfaces. Geometrical optimizations were achieved by relaxing all ionic positions and supercell vectors until the Hellman-Feynmann forces were less than 0.02 eV $Å^{-1}$. The dispersion correction was also considered in this study by using the DFT-D3 method.[7] The slab method was used to model pristine and Cr-doped Ni_2P surfaces with surface-bulk-like interactions. For (300) surfaces, relaxation of the atomic coordinates in the seven uppermost layers and fixation of the atomic coordinates in the four bottom layers were done; whereas, for (111) surfaces, relaxation of the atomic coordinates in the ten uppermost layers and fixation of the atomic coordinates in the five bottom layers were done. A vacuum region of 20 Å was introduced in the direction of the z-axis to avoid interactions between periodic images. Free energy diagrams for the MOR and HER pathways considered TΔS and ZPE corrections for CO_2 and H_2.

Supplementary Figures and Tables

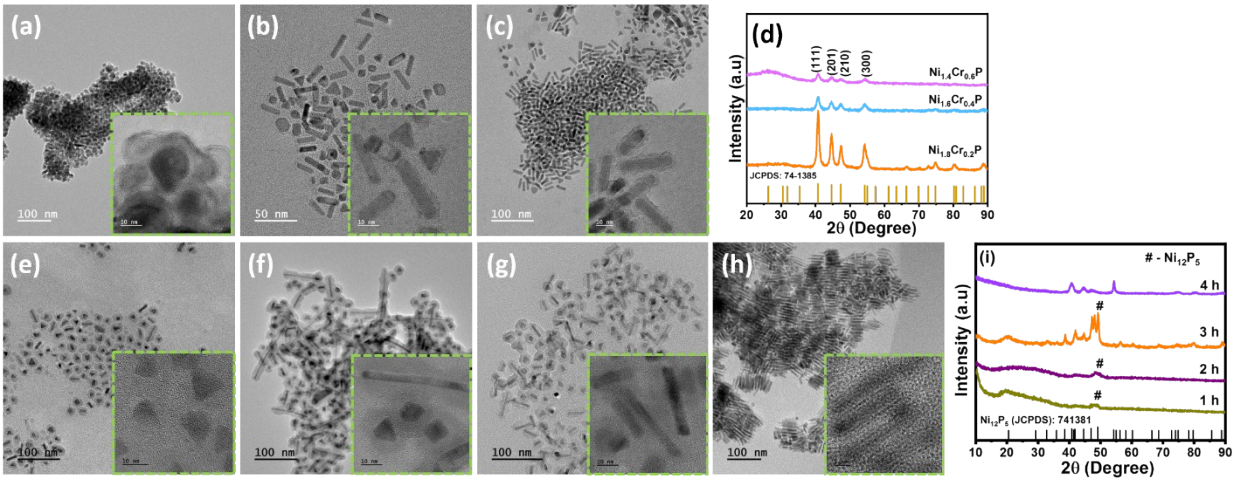

Figure S1. High resolution TEM & HR-TEM images of (a) $Ni_{1.4}Cr_{0.6}P$, (b) $Ni_{1.6}Cr_{0.4}P$ (c) $Ni_{1.8}Cr_{0.2}P$ and (d) their corresponding XRD patterns. High-resolution TEM & HR-TEM images of $Ni_{1.2}Cr_{0.8}P$ synthesized at 320 ^{o}C for (e) 1 h, (f) 2 h, (g) 3 h (h) 4 h and (i) their corresponding XRD patterns.

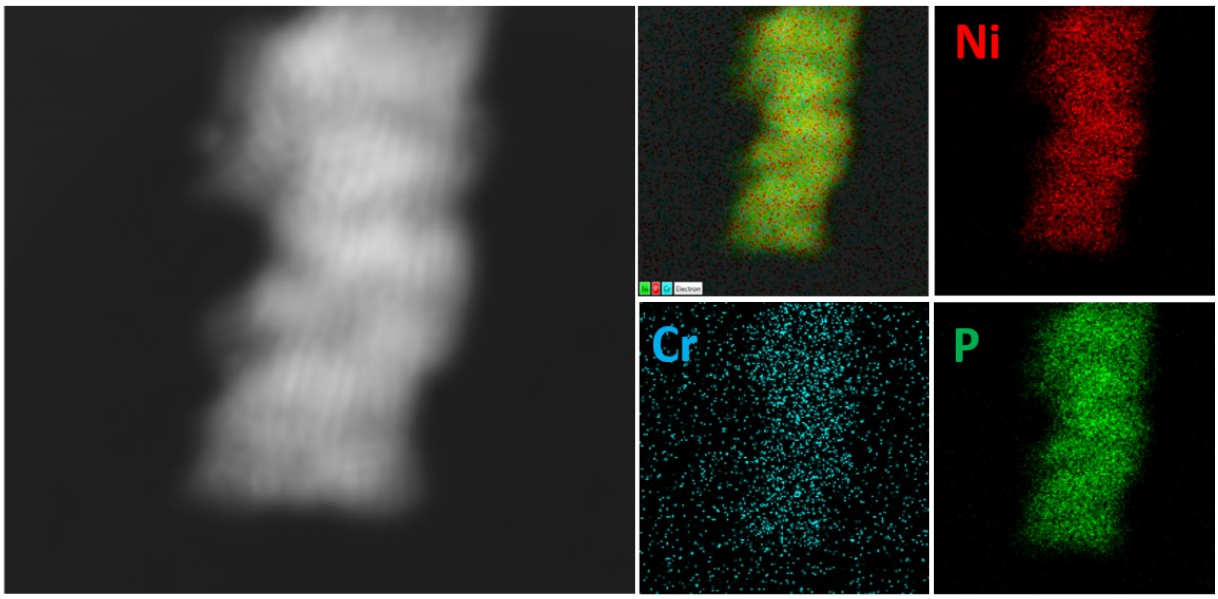

Figure S2. STEM image and EDS elemental mapping of $Ni_{1.2}Cr_{0.8}P$ NCs.

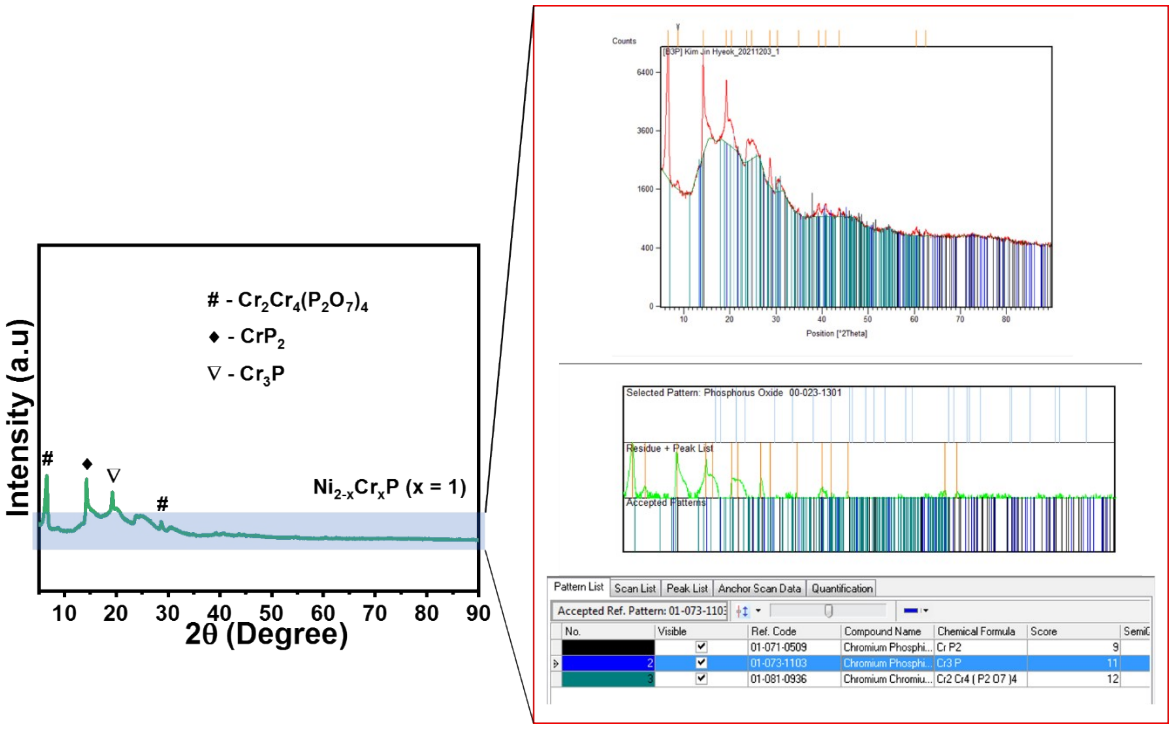

Figure S3. XRD pattern of $Ni_{2-x}Cr_xP$ (x = 1) analyzed using X'pert High Score software.

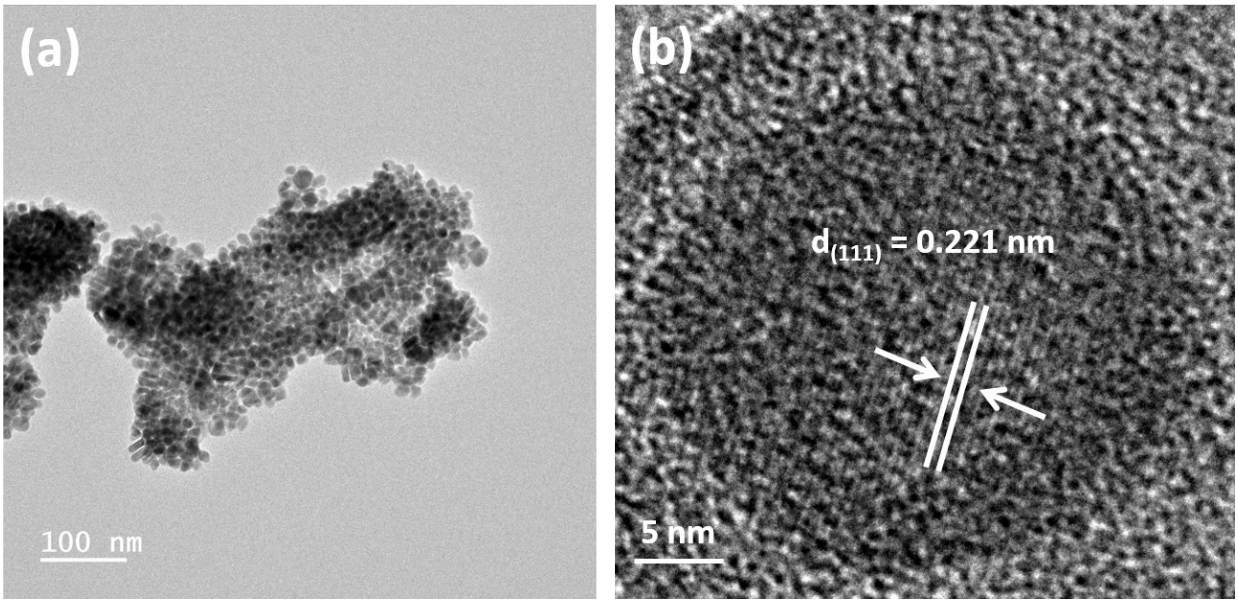

Figure S4. (a) TEM and (b) HR-TEM images of $Ni_{1.2}Cr_{0.8}P$ NCs using $Cr(NO_3)_3$ precursor.

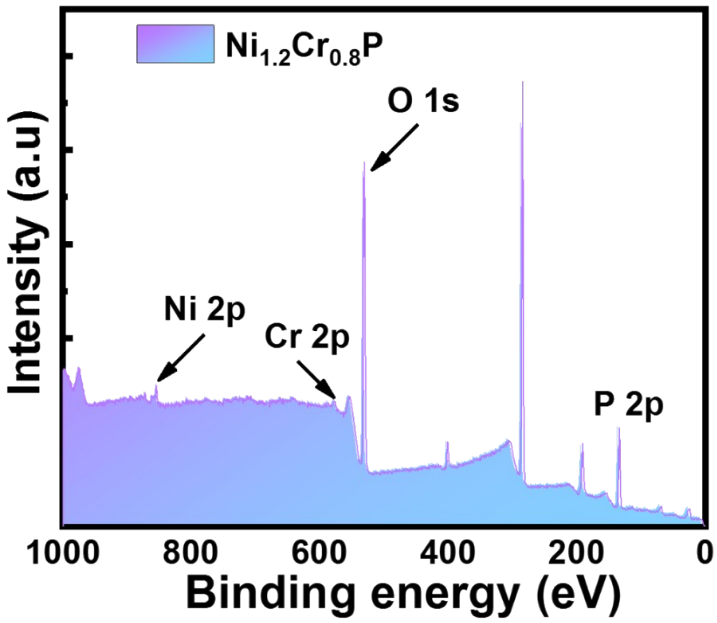

Figure S5. The high-resolution survey spectrum of $Ni_{1.2}Cr_{0.8}P$ NRs confirms all the elements including Ni, Cr, P and O. In addition, the minor peaks at 200, 280 and 400 eV correspond to Cl, C, and N, respectively.

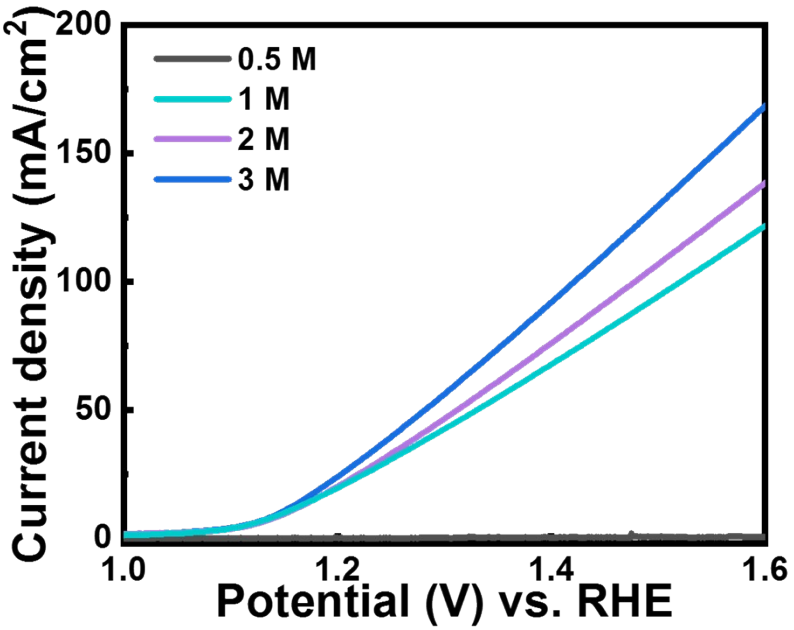

Figure S6. MOR polarizations curves for $Ni_{1.2}Cr_{0.8}P$ electrocatalyst measured in different MeOH concentrations.

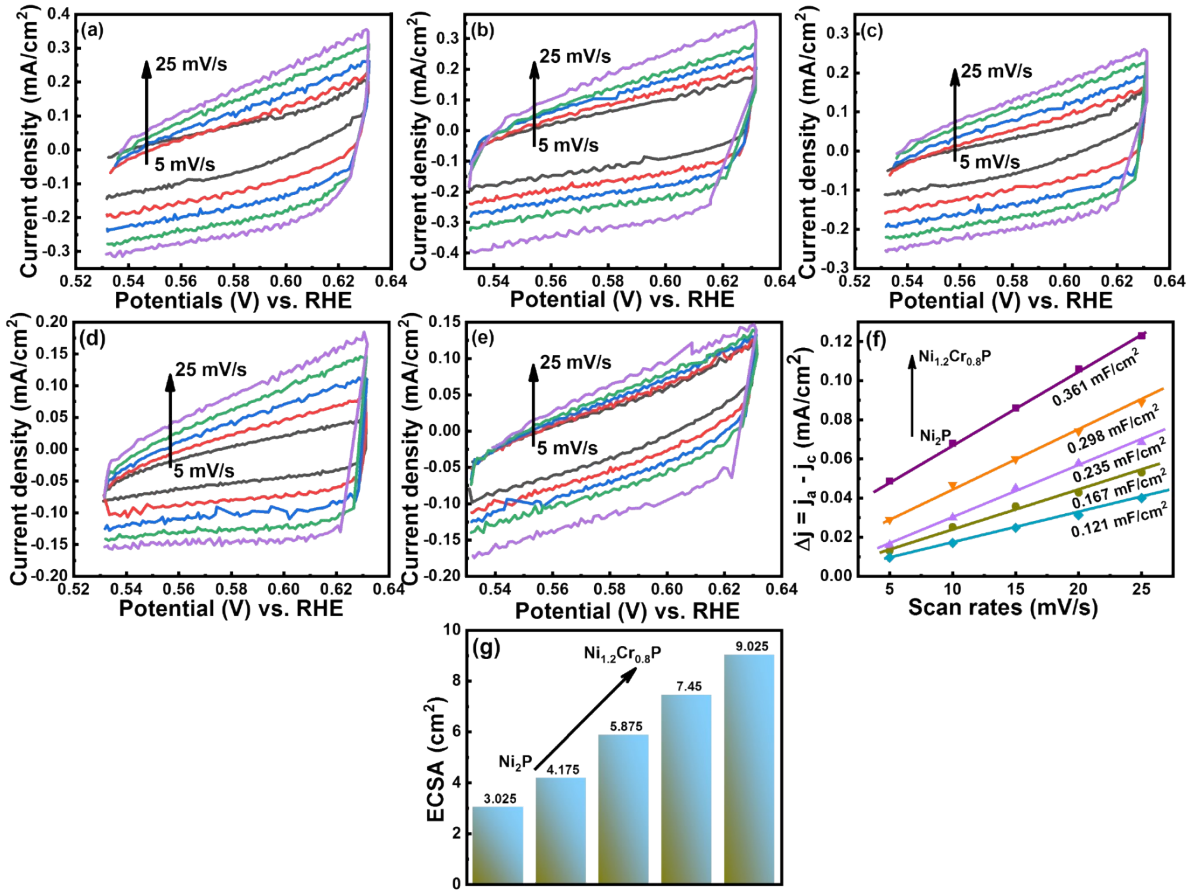

Figure S7. Cyclic Voltammograms (CVs) of (a) $Ni_{1.2}Cr_{0.8}P$, (b) $Ni_{1.4}Cr_{0.6}P$, (c) $Ni_{1.6}Cr_{0.4}P$, (d) $Ni_{1.8}Cr_{0.2}P$ and (e) Ni_2P. (f) Double-layer capacitance (C_{dl}) of the electrocatalysts. (g) Electrochemical active surface area (ECSA) of the electrocatalysts.

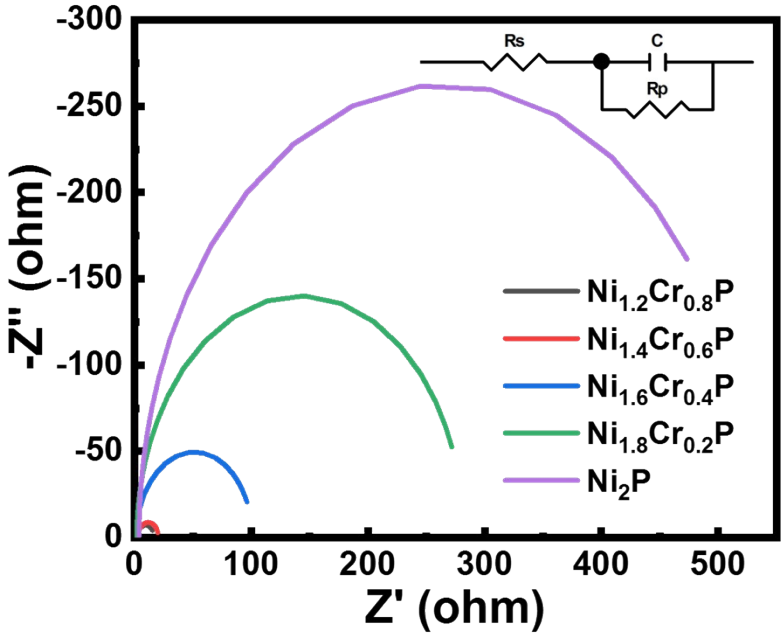

Figure S8. Nyquist plots of $Ni_{2-x}Cr_xP$ electrocatalysts. Inset shows the equivalent circuit with applied series resistance used for EIS study. Applying series resistance helps in reducing the effects of contact resistance between the electrodes and the catalysts material and ensures reliable EIS data. Including series resistance also compensates solution resistance that interferes with the interpretation of impedance data and provides better correction and analysis of electrochemical properties of the catalysts. Moreover, authors believe that the applied series resistance facilitates the fitting of electrical equivalent circuit models to the experimental impedance data and enables more accurate characterizations of the catalyst's electrochemical behavior.[8,9]

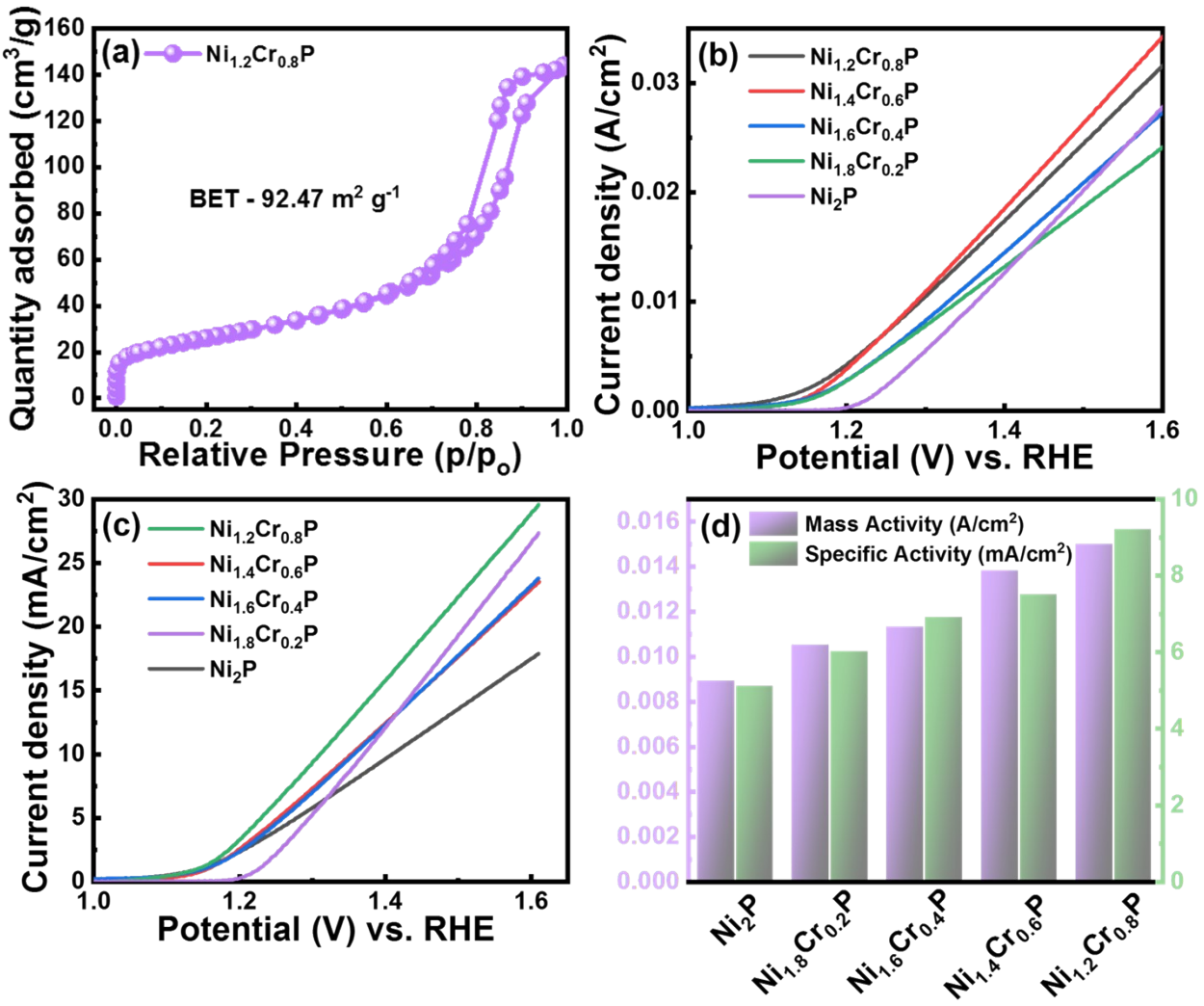

Figure S9. (a) BET measurement of $Ni_{1.2}Cr_{0.8}P$ electrocatalysts. (b) MOR polarization curves of electrocatalysts normalized with mass activity. (c) MOR polarizations curves of electrocatalyst normalized with ECSA. (d) comparison of mass activity and specific activity of electrocatalysts for MOR.

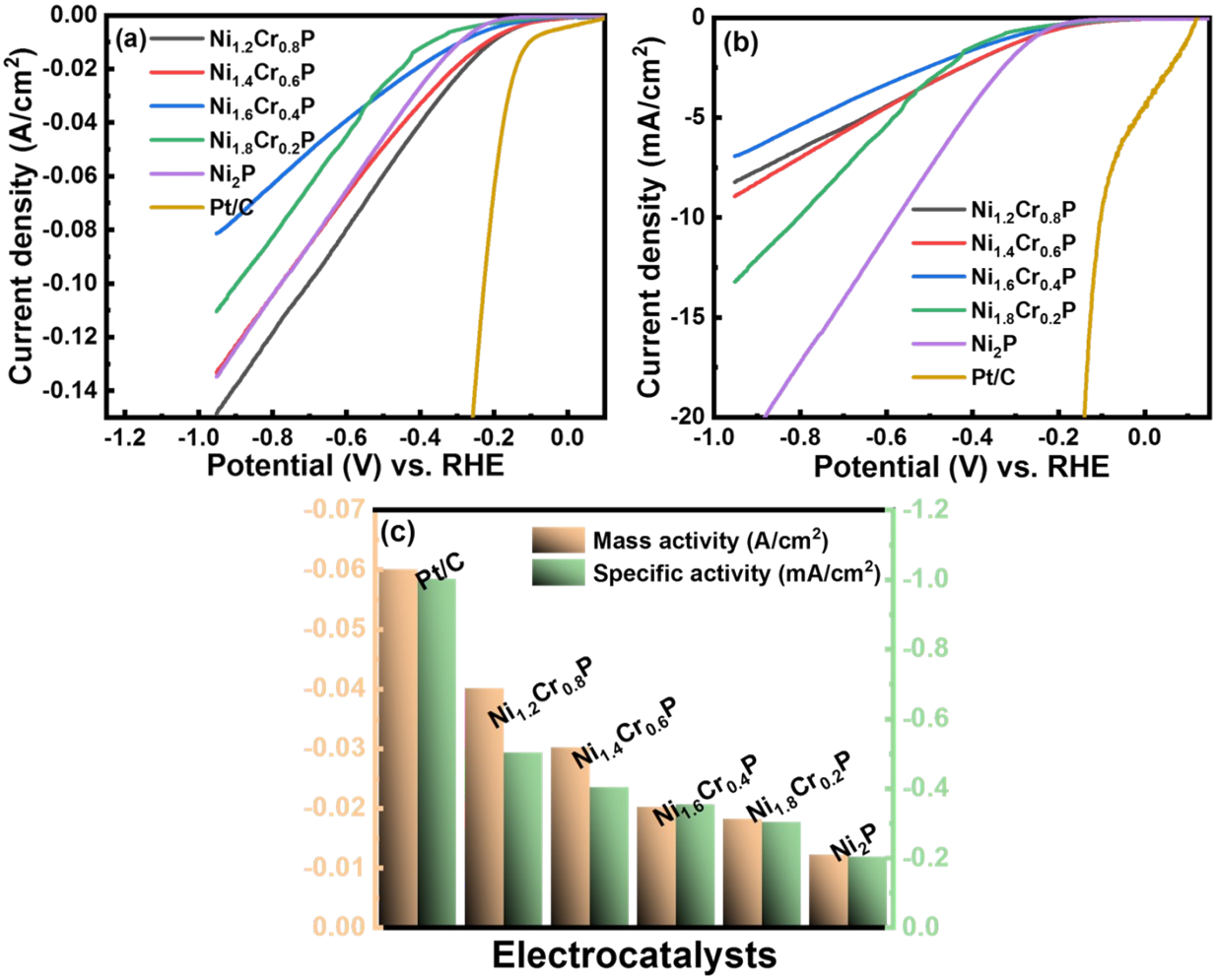

Figure S10. (a) HER polarization curves of electrocatalysts normalized with mass activity. (b) HER polarizations curves of electrocatalyst normalized with ECSA. (c) Comparison of mass activity (MA) and specific activity (SA) of electrocatalysts for HER.

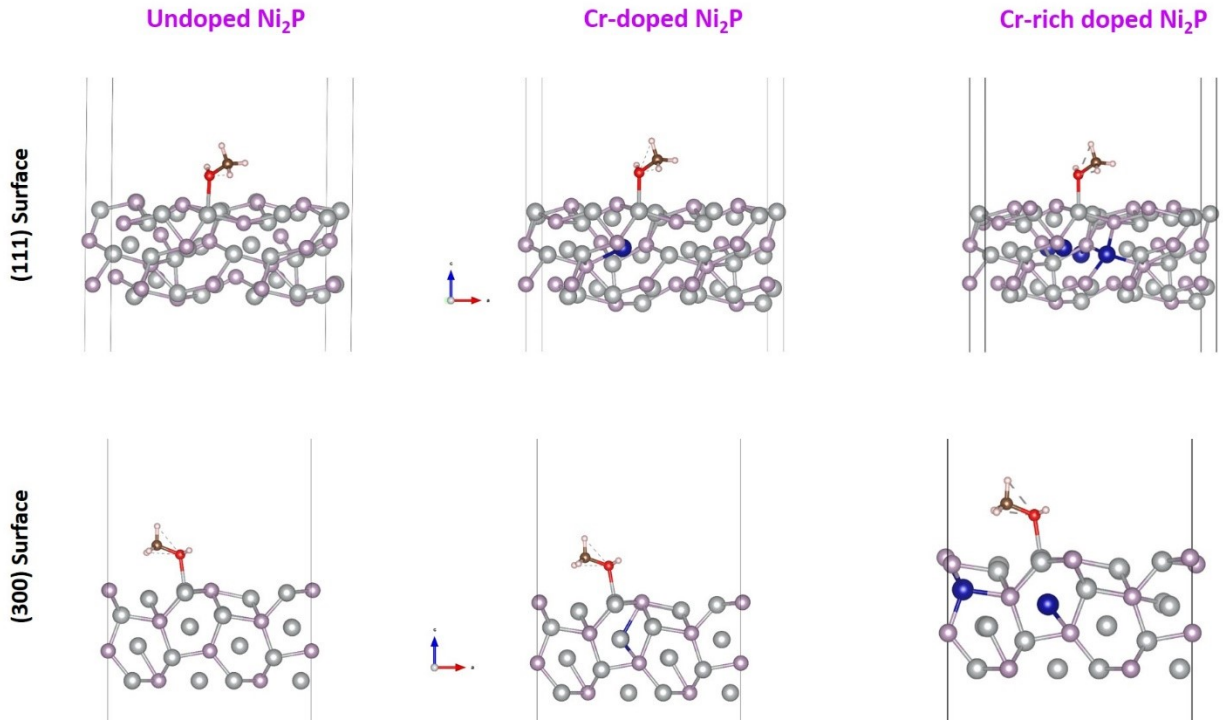

Figure S11. Optimized structural models for DFT calculations

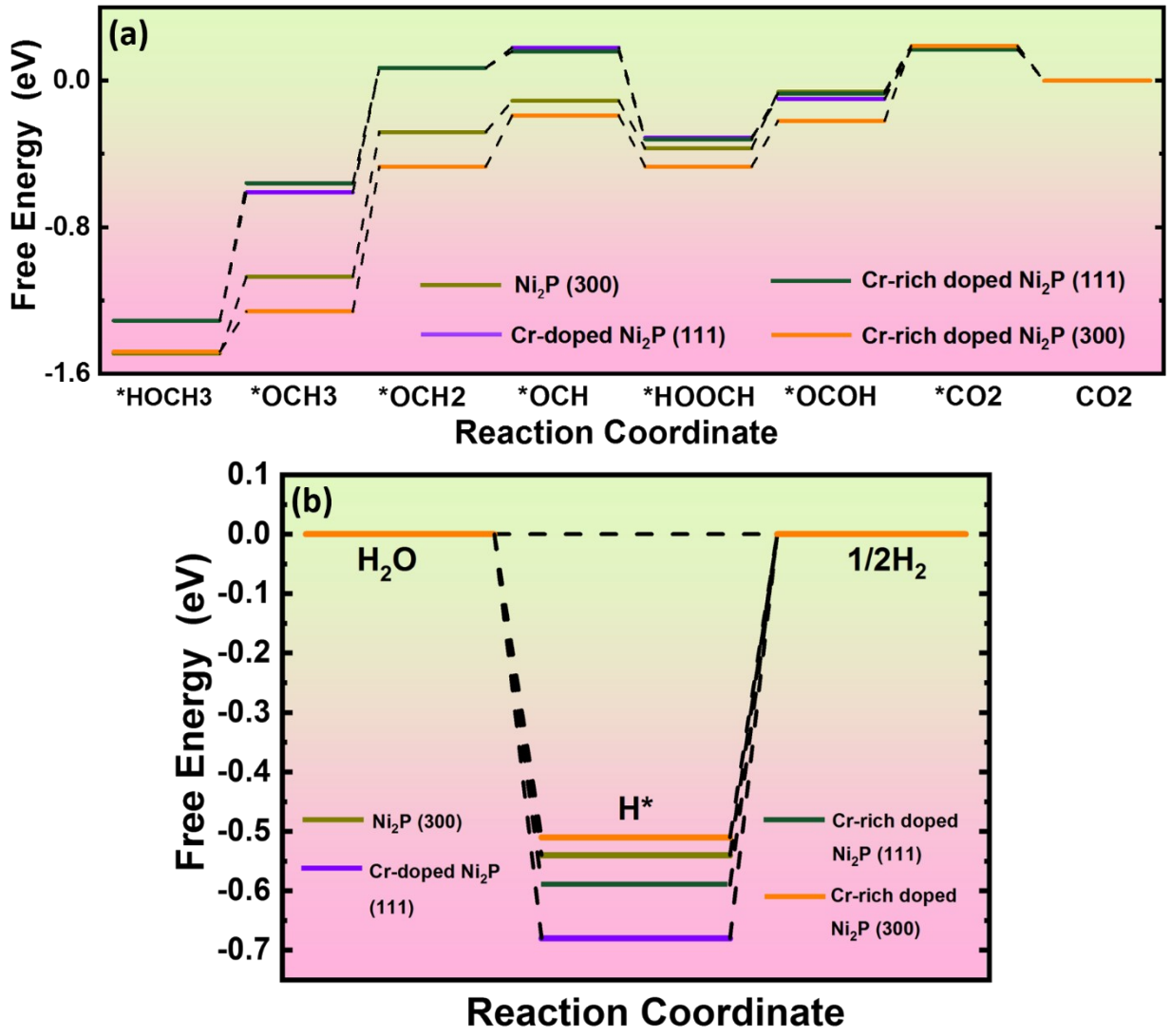

Figure S12. Free energy diagrams (a) Gibbs free energy diagrams of undoped Ni_2P (300), Cr-doped Ni_2P (111), Cr-rich doped Ni_2P (111) and Cr-rich doped Ni_2P (300) for MOR. (b) Hydrogen adsorption free energy diagrams of undoped Ni_2P (300), Cr-doped Ni_2P (111), Cr-rich doped Ni_2P (111) and Cr-rich doped Ni_2P (300) for HER.

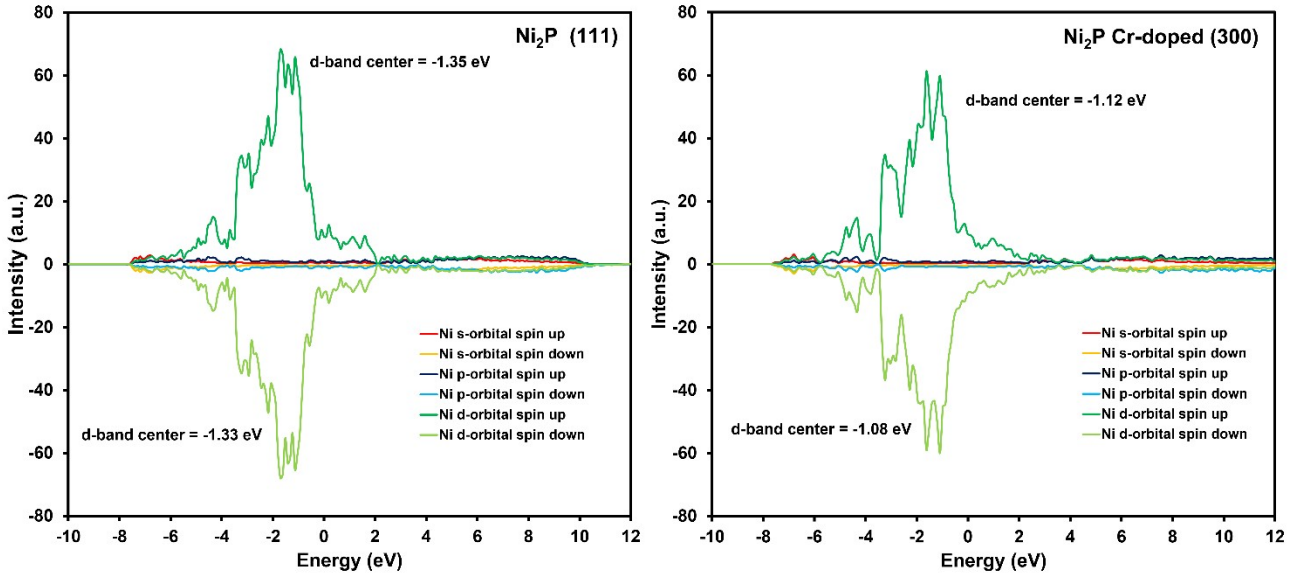

Figure S13. Projected Density of States (PDOS) of Nickel atoms in Ni_2P (111) surface (left) and Ni_2P Cr-doped (300) surface (right).

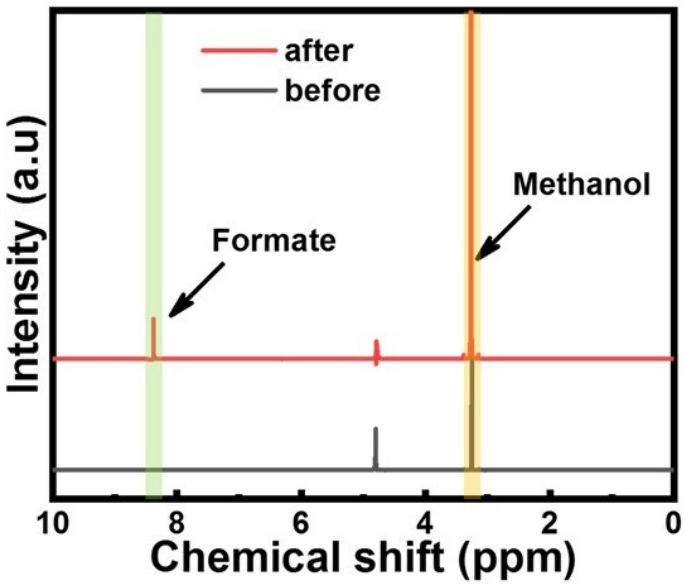

Figure S14. Methanol oxidation product analysis using NMR technique.

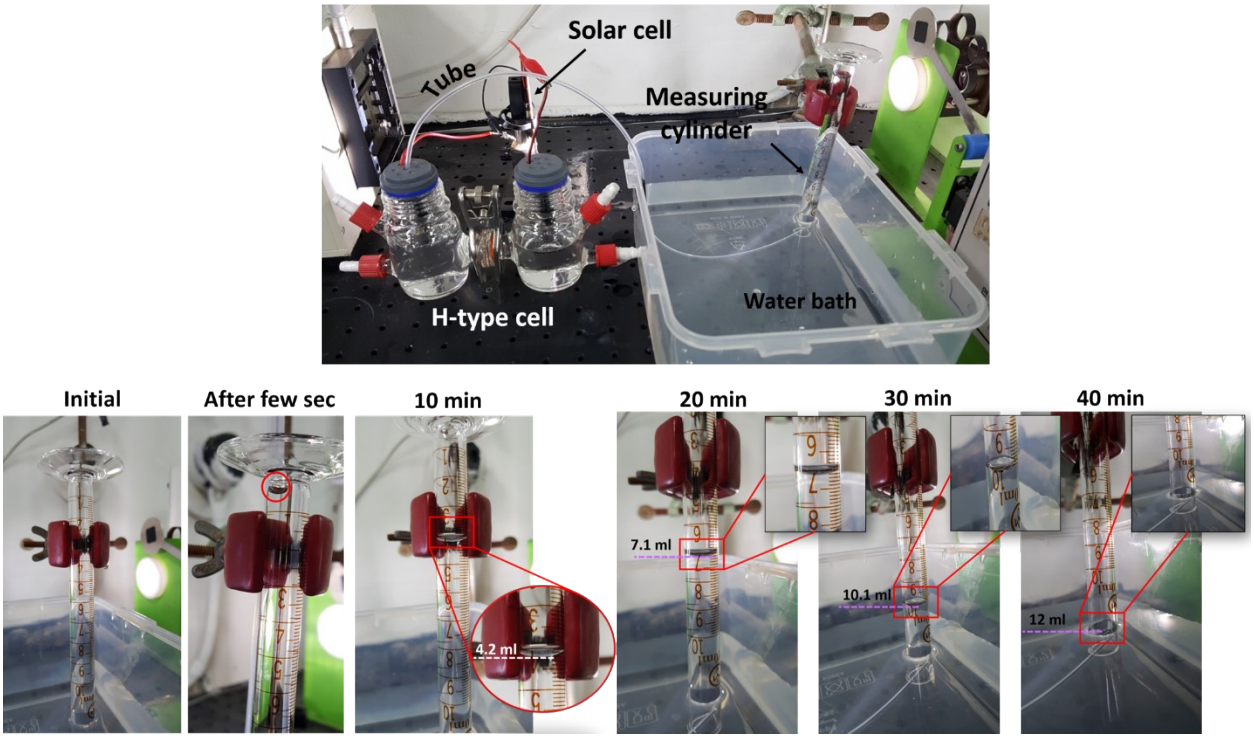

Figure S15. Collection of H_2 gas evolved during 40 min. of electrolysis process using a conventional water drainage method.

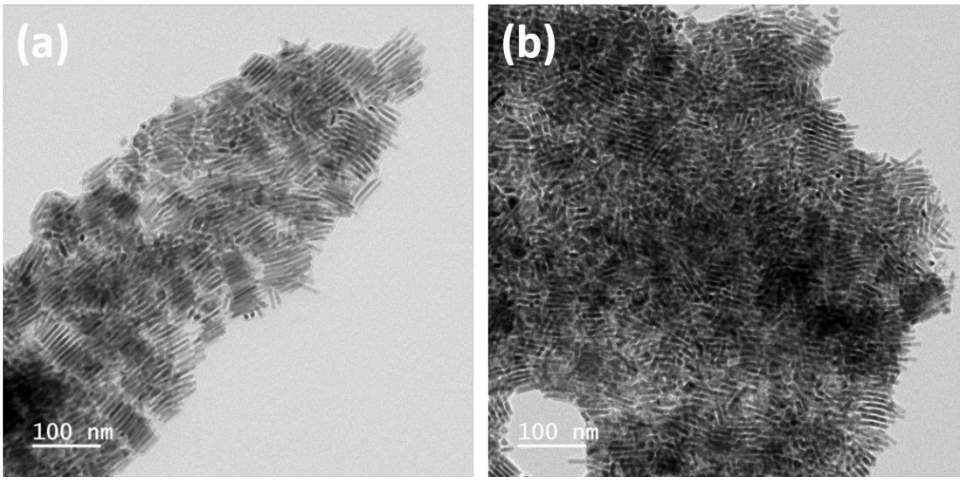

Figure S16. High-resolution TEM images of $Ni_{1.2}Cr_{0.8}P$ electrocatalysts after (a) MOR process and (b) HER process.

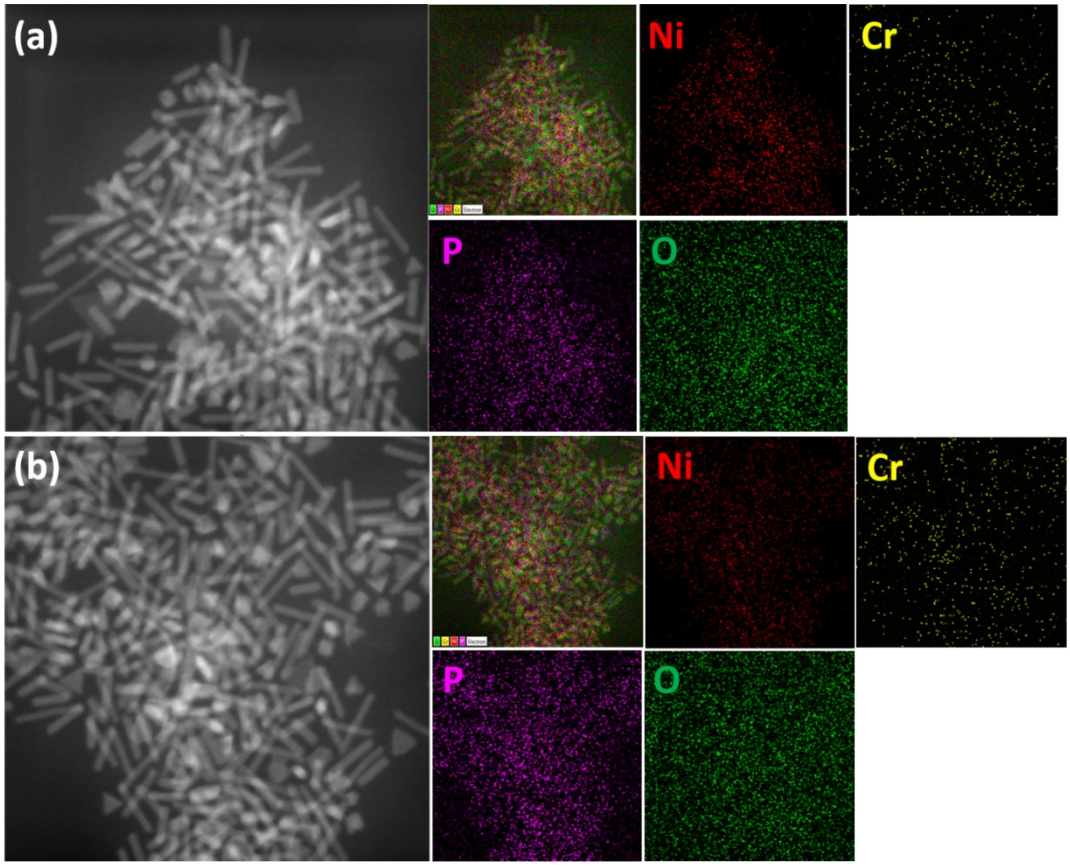

Figure S17. Post-electrolysis EDS elemental mapping of $Ni_{1.2}Cr_{0.8}P$ NRs after (a) MOR process and (b) HER process.

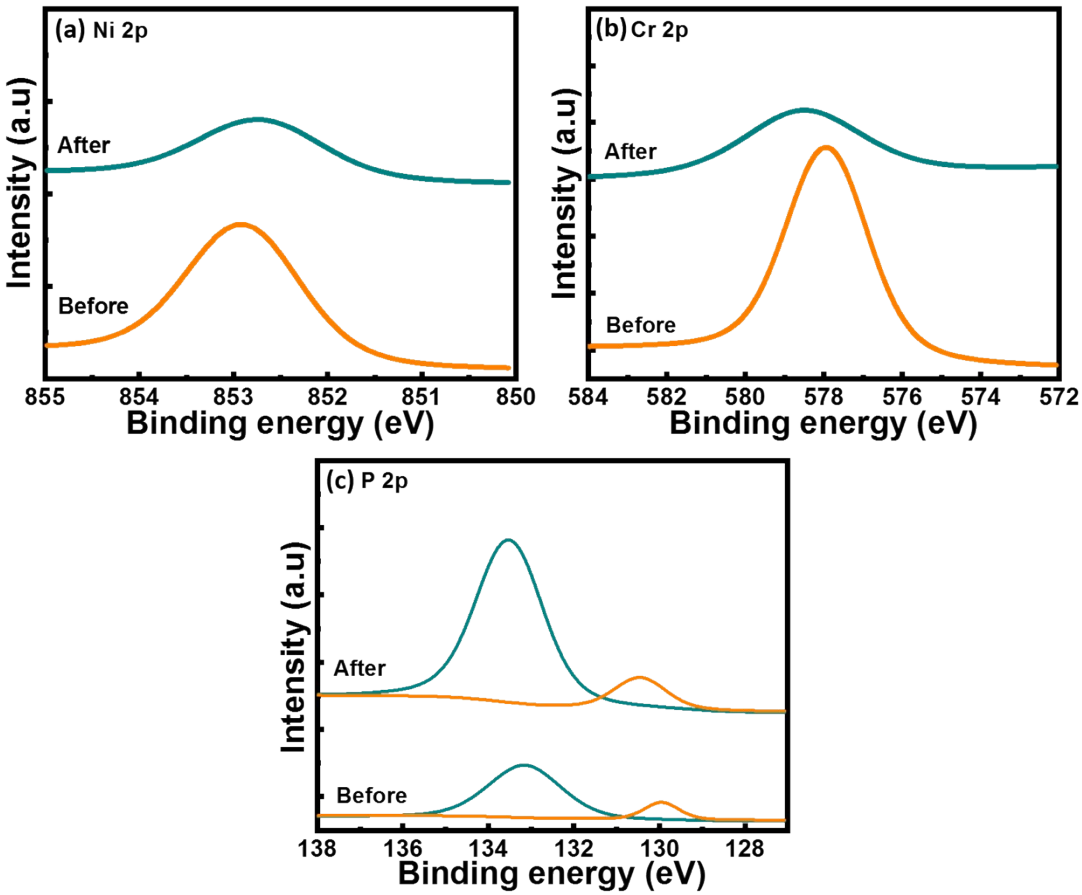

Figure S18. High-resolution core-level spectra of (a) Ni 2p, (b) Cr 2p and (c) P 2p before and after MOR process.

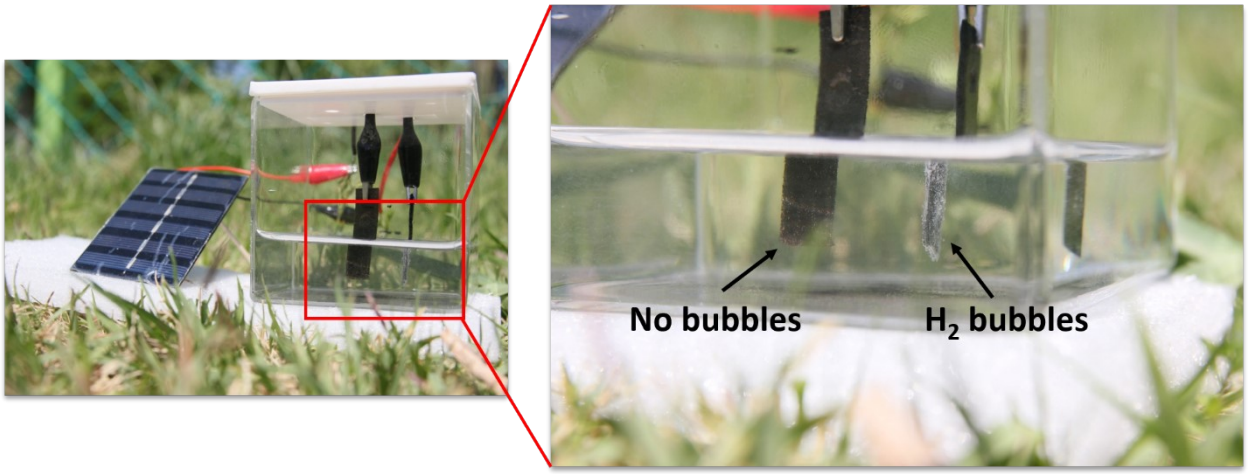

Figure S19. Digital photographs of solar-driven electrolysis under natural sunlight.

Table S1. Composition of Ni_2P and Cr-doped Ni_2P from ICP-OES.

Catalysts	Ni (at%)	Cr (at%)	P (at%)
Ni_2P	62.3	-	37.7
Cr-doped Ni_2P	40.62	27.08	32.3

Table S2. Comparison of OMeS cell voltage with other recently reported catalysts.

Electrocatalyst	Electrolyte	Catalyst type	Overpotential (mV) at η	References
$Ni_{1.2}Cr_{0.8}P$	**1.0 M KOH + 3 M MeOH**	**Powder**	**1.14@10**	**This work**
CuCo-UMOFNF	1.0 M KOH + 3 M MeOH	Substrate	1.36@10	10
NiIr-MOF/NF	1.0 M KOH + 4 M MeOH	Substrate	1.39@10	11
$Ni(OH)_2$/NF	1.0 M KOH + 0.5 M MeOH	Substrate	1.36@100	12
Co_xP@NiCo-LDH/NF	1.0 M KOH + 0.5 M MeOH	Substrate	1.43@10	13
$Ni_{0.33}Co_{0.67}(OH)_2$/NF	1.0 M KOH + 0.5 M MeOH	Substrate	1.50@10	14
$Co(OH)_2$@HOS/CP	1.0 M KOH +	Substrate	1.50@10	15

	3 M MeOH			
$Co\text{-}Rh_2$	1.0 M KOH + 1.0 M MeOH	Substrate	1.54@10	16
Pt-CoSe/NC	0.5 M H_2SO_4 + 1.0 MeOH	Substrate	0.67@10	17
Co-CuO	1.0 KOH + 1.0 MeOH	Substrate	1.51@10	18
$Os–Ni_xP/N–C/NF$	1.0 KOH + 1.0 MeOH	Substrate	1.43@10	19
$Mo\text{-}Co_4N$	1.0 KOH + 1.0 MeOH	Substrate	1.42@10	20

References

[1] G. J. Conibeer and B. S. Richards, *Int. J. Hydrogen Energy*, **2007**, *32*, 2703–2711.

[2] G. Kresse, J. Furthmuller, *Computational Mater. Sci.* **1996**, *6*, 1, 15-50.

[3] G. Kresse, J. Furthmuller, *Phys Rev B Condens Matter.* **1996,** *54*, 16, 11169.

[4] P. E. Blochl, *Phys Rev B Condens Matter.* **1994**, *50*, 24, 17953.

[5] G. Kresse, D. Joubert, *Physical Review B,* **1999**, *59*, 3, 1758.

[6] J. P. Perdew, K. Burke, M. Ernzerhof, *Phys. Rev. Lett.* **1996**, *77*, 18, 3865.

[7] S. Grimme, J. Antony, S. Ehrlich, H. Krieg, *J. Chem. Phys.* **2010,** *132*, 15, 154104.

[8] T. Pajkossy and R. Jurczakowski, *Curr. Opinion Electro.*, 2017, **1**, 1, 53-58

[9] N. O. Laschuk, E. B. Easton and O. V. Zenkina, *RSC Adv.*, 2021, **11**, 27925-27936.

[10] X. Wei, S. Wang, Z. Hua, L. Chen, J. Shi, *ACS Appl. Mater. Interfaces* **2018**, *10*, 25422-25428.

[11] Y. Xu, M. Liu, M. Wang, T. Ren, K. Ren, Z. Wang, X. Li, L. Wang, H. Wang, *Appl. Catal. B. Environ.* **2022**, *300*, 120753.

[12] J. Hao, J. Liu, D. Wu, M. Chen, Y. Liang, Q. Wang, L. Wang, X.-Z. Fu and J.-L. Luo, *Appl. Catal. B: Environ.*, **2021**, *281*, 119510.

[13] M. Li, X. Deng, Y. Liang, K. Xiang, D. Wu, B. Zhao, H. Yang, J.-L. Luo and X.-Z. Fu, *J. Energy Chem.*, **2020**, *50*, 314-323.

[14] M. Li, X. Deng, K. Xiang, Y. Liang, B. Zhao, J. Hao, J. L. Luo and X. Z. Fu, *ChemSusChem*, **2020**, *13*, 914-921.

[15] K. Xiang, D. Wu, X. Deng, M. Li, S. Chen, P. Hao, X. Guo, J. L. Luo and X. Z. Fu, *Adv. Funct. Mater.*, ***2020***, *30*, 1909610.

[16] Y. Guo, X. Yang, X. Liu, X. Tong and N. Yang, *Adv. Energy Mater.*, 2023, **33**, 2, 2209134.

[17] Y. Zhou, Q. Wang, X. Tian and L. Feng, *Nano Res.,* 2022, **15**, 8936-8945.

[18] S. Jung, R. A. Senthil, A. Min, A. Kumar, C. J. Moon and M. Y. Choi, *Small Methods*, 2024, https://doi.org/10.1002/smtd.202301628

[19] Z. Duan, T. Ren, Q. Mao, H. Yu, K. Deng, Y. Xu, Z. Wang, L. Wang and H. Wang, *J. Mater. Chem. A*, 2022, **10**, 18126-18131.

[20] T. Wang, X. Cao, H. Qin, X. Chen, J. Li and L. Jiao, *J. Mater. Chem. A*, 2021, 9, 21094-21100.